Received: 10 May 2024 | Revised: 9 October 2024 | Accepted: 10 November 2024

DOI: 10.1111/ijac.15003

International Journal of Applied Ceramic Technology

RESEARCH ARTICLE

Physical characterization of composites based on yttria-stabilized zirconia and doped lanthanum gallate

Talita G. Fujimoto[1] | **V. Seriacopi**[2,3] | **Izabel F. Machado**[3] | **Reginaldo Muccillo**[1] | **Eliana N. S. Muccillo**[1]

[1]Center of Science and Technology of Materials, Energy and Nuclear Research Institute-IPEN, Sao Paulo, Brazil

[2]Mechanical Engineering Department, Maua Institute of Technology, Sao Paulo, Brazil

[3]Mechatronics and Mechanical Systems Engineering Department, Escola Politécnica, University of São Paulo, Sao Paulo, Brazil

Correspondence
Eliana N. S. Muccillo, Center of Science and Technology of Materials, Energy and Nuclear Research Institute-IPEN, 05508-000, Sao Paulo, Brazil.
Email: enavarro@usp.br

Funding information
FAPESP, Grant/Award Number: 2013/07692-2; CNPq, Grant/Award Numbers: 305557/2022-0, 306894/2023-8; CAPES, Grant/Award Number: 0001; CNEN

Abstract

This work reports a systematic study on the microstructure, electrical conductivity, and nanoindentation of 8 mol% yttria-stabilized zirconia (8YSZ), $La_{0.9}Sr_{0.1}Ga_{0.8}Mg_{0.2}O_{3-\delta}$ (LSGM) in both pure form and as composites. The main purpose was to evaluate the effects of the minor phase on the properties of the composite materials. Commercial 8YSZ was the major phase. Pure LSGM and composites consisting of 1, 10, and 20 wt.% LSGM were prepared by the solid-state reaction method. Sintering experiments were carried out from 1200°C to 1450°C. The temperature of maximum shrinkage decreased with increasing LSGM content. The average grain size of the composites was dependent on the relative proportion of the minor phase. Interface reactions occurr during sintering. Electrical conductivity of the composites was found to be lower compared to that of 8YSZ. The hardness showed no significant variation with the minor phase content, although a beneficial effect on the elastic modulus was noted for composites containing 10 wt.% LSGM.

KEYWORDS
composites, electrical conductivity, LSGM, microstructure, nanoindentation, yttria-stabilized zirconia

1 | INTRODUCTION

Stabilized zirconia containing 8 mol% yttria (8YSZ) with a cubic fluorite-type structure is an oxygen ion conductor with applications in electrochemical devices, such as solid oxide fuel cells (SOFCs) for clean-energy production.[1,2] In addition to its high ionic conductivity, 8YSZ exhibits good chemical stability over wide range of oxygen partial pressure, and it is the ideal solid electrolyte for SOFCs operating at high temperatures (~800 to ~1000°C). The mechanical strength of 8YSZ is suitable for technological applications, but it is lower than that of 3 mol% yttria-stabilized zirconia, 3YSZ.[3]

Lanthanum gallate with partial replacement of strontium and magnesium for lanthanum and gallium, respectively, is a well-known oxygen ion conductor with higher ionic conductivity than that of 8YSZ, and has been proposed for substituting 8YSZ in SOFCs operating in the intermediate-temperature range (~600 to ~800°C).[4] Besides the high ionic conductivity of doped-lanthanum gallates, this solid electrolyte display a wide electrolytic domain. The elastic properties of solid electrolytes based on lanthanum gallate were shown to depend on the relative amounts of strontium and magnesium in the lanthanum gallate matrix. Some mechanical properties of doped-lanthanum gallates were summarized in a recent review.[5]

Former studies on composite ceramic materials for SOFCs revealed improved performance on diverse properties, such as reduction of carbon contamination, decrease

in the area specific resistance, and increase in the electrical conductivity.[6–8] Some recent reports also reveal that secondary phases may be formed during sintering at high temperatures and influence the electrical conductivity of the composites.[9,10]

Composite ceramics based on 8YSZ have received increasing attention as solid electrolytes and electrodes in SOFCs,[3,11–14] and as thermal barrier coating.[15,16] The electrical and mechanical properties of the composite electrolyte based on 8YSZ and 3YSZ, for instance, revealed increased fracture toughness accompanied by a slight increase in electrical conductivity.[17] An increase in electrical conductivity was also reported for 94 wt.% 8YSZ-6 wt.% $La_{9.33}Si_6O_{26}$ composites synthesized via a chemical route.[11] Composites of 8YSZ and samaria-doped ceria (SDC) revealed an increase in electrical conductivity with increasing amounts of SDC up to a ratio of 8.5:1.5 (in wt.%).[13] A suitable thermal expansion coefficient, along with a dual structure was reported for composites of 8YSZ and Bi_2O_3.[18] Reduction of the sintering temperature to about 900°C–1000°C was also found for yttria-stabilized zirconia with Bi_2O_3 addition.[19]

It is well-recognized that lanthanum diffusion accounts for lanthanum zirconate formation whenever compounds containing zirconium and lanthanum are combined. This reaction is responsible for degradation of the electrical and mechanical properties of the compounds and has been investigated especially for cathodes in solid oxide fuel cells.[20,21]

In a previous study, 8YSZ was added as a minor phase (up to 20 wt.%) to doped-lanthanum gallate to form composites envisaging to improve the microstructure of the major phase and their microstructure-dependent properties. In that case, an improvement of the microstructure was obtained up to 10 wt.% addition of 8YSZ, due to a reduction of the fraction of the usually found secondary phases in doped-lanthanum gallate. Chemical reaction of the two solid electrolytes was observed for higher contents of the minor phase, leading to formation of the lanthanum zirconate phase. In addition, an unexpected increase in the bulk conductivity and a decrease in the activation energy for conduction were obtained for 1 wt.% addition of 8YSZ.[22]

In this work, the effects of $La_{0.9}Sr_{0.1}Ga_{0.8}Mg_{0.2}O_{2-\delta}$ (hereafter referred to as LSGM) addition on densification, microstructure, electrical and mechanical properties of 8YSZ were investigated. The main purpose was to obtain composite ceramics with improved ionic conductivity without or with little degradation of other properties of 8YSZ.

2 | EXPERIMENTAL

2.1 | Materials

The starting materials were zirconia-8 mol% yttria (8YSZ, 99.6%, Tosoh), lanthanum oxide (La_2O_3, 99.9%, Alfa Aesar), gallium oxide (Ga_2O_3, 99.99%, Alfa Aesar), strontium carbonate ($SrCO_3$, 99.99%, Alfa Aesar), and magnesium oxide (MgO, P.A., Merck).

2.2 | Sample preparation

The $La_{0.9}Sr_{0.1}Ga_{0.8}Mg_{0.2}O_{3-\delta}$ electrolyte was synthesized according to the method previously described.[23] In brief, the starting materials were dried at 100°C, except for the lanthanum precursor, which was heat treated at 1000°C for 3 h. Then, stoichiometric amounts of each material were mixed together and calcined at 1250°C for 4 h followed by deagglomeration. This step was repeated up to 12 h of total calcination time. After calcination, the mixed powder was attrition milled for 1 h with zirconia balls (ϕ 2 mm, YTZP, Tosoh) in an alcoholic medium and dried in an oven. The prepared LSGM powder consists of soft agglomerates of 1–5 μm in size. Other characteristics of the prepared LSGM powder may be found in a previous publication.[23] The typical particle size of 8YSZ is 40 nm (supplier information). Solid electrolytes of (100-x) 8YSZ + x LSGM, with $x = 0$, 1, 10 and 20 wt.% were prepared by the solid-state reaction method. Hereafter, composites will be denoted according to the fraction of the minor phase as: 1LSGM, 10LSGM and 20LSGM. The 8YSZ and LSGM powders were mixed in the desired proportions in an agate mortar with isopropyl alcohol until drying. The mixtures were pressed into disc-shaped pellets in a stainless-steel dye (ϕ 8 and 2 mm thickness) at 50 MPa. Sintering experiments were carried out in a resistive furnace (Lindberg, BlueM) at dwell temperatures in the 1200°C–1450°C range for a fixed dwell time of 4 h.

2.3 | Characterization

Linear shrinkage measurements were performed in a push-rod vertical dilatometer (Anter, Unitherm 1161) up to 1500°C with 10°C.min^{-1} heating rate. The apparent density of sintered specimens was determined using the Archimedes method with distilled water. The density of the composites was calculated taking into account the crystallographic densities and volume fractions of 8YSZ and LSGM. Crystalline phases were evaluated by

conventional X-ray diffraction (XRD) analysis (Bruker-AXS, D8 Advance) with Cu k_α radiation in the $20° \leq 2\theta \leq 80°$ range, 0.05° step size and 3 s counting time. The microstructure of the sintered ceramics was evaluated by field emission gun scanning electron microscopy (SEM) (FEI, Inspect F50) on the polished and thermally etched (100°C below the sintering temperature for 30 min) surfaces of the pellets. Complementary microstructure analysis was carried out on specific microregions of sintered samples by energy dispersive spectroscopy (EDS).

Electrochemical impedance spectroscopy technique was utilized for measuring the electrical response of the ceramics either pure or composites. An AC signal was applied to ceramic pellets in the 250°C to 500°C range. Measurements were carried out in the ambient atmosphere ($pO_2 = 0.21$ atm) using an impedance analyzer (HP, 4192A) in the 5–13 MHz range, with input signal of 200 mV, and ~60 min after the measuring temperature has been attained for ensuring thermal equilibration of the pellets. The measured impedance in the Nyquist plan Z = Z' + iZ'', where Z' and Z'' are the real and imaginary components of the total impedance, respectively, was analyzed based on equivalent electric circuit elements by software.[24] Silver electrodes were applied by painting onto large surfaces of pellets and curing at 400°C. The electrical conductivity of the bulk was calculated from experimentally determined resistances, and the Arrhenius plots were obtained by Equation (1):

$$\sigma = \sigma_0 \exp\left[-\frac{E_a}{kT}\right], \tag{1}$$

where, σ_0, E_a, k and T are the pre-exponential factor, the activation energy for conduction, the Boltzmann constant and the absolute temperature, respectively.

Nanoindentation tests were performed with a triboindenter (Bruker, Hysitron TI 950) under maximum loads of 4 and 8 mN, with loading, holding, and unloading stages each lasting for 5 s. A diamond indenter with Berkovich geometry was applied during tests. Load–displacement curves (P–h curves) were obtained for the samples. Reduced modulus and indentation hardness can be predicted taking the data to be analyzed by the Oliver–Pharr algorithm.[25] In addition, the sample elastic modulus (E) was calculated based on the reduced modulus (E_r) and indenter elastic modulus (E_i), and respective influences of Poisson ratios (ν) according to Equation (2), assuming for the diamond the elastic modulus equal to 1140 GPa and Poisson ratio of 0.07[25]:

$$\frac{1}{E_r} = \frac{\left(1-\upsilon_i^2\right)}{E_i} + \frac{\left(1-\upsilon_s^2\right)}{E} \tag{2}$$

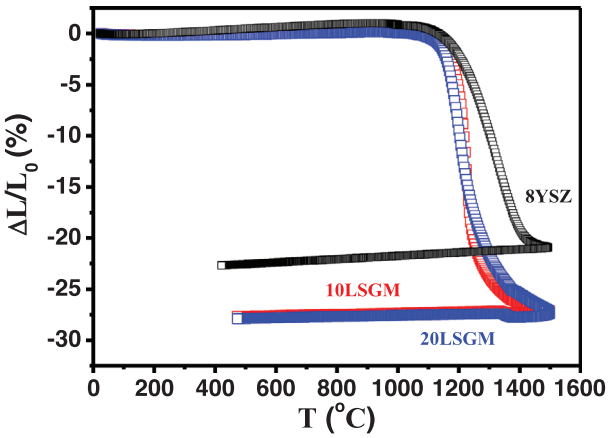

FIGURE 1 Linear shrinkage curves of pure 8 mol% yttria-stabilized zirconia (8YSZ), and 10 mol% $La_{0.9}Sr_{0.1}Ga_{0.8}Mg_{0.2}O_{3-\delta}$ (LSGM) and 20LSGM composites.

3 | RESULTS AND DISCUSSION

3.1 | Densification

Figure 1 shows linear shrinkage curves up to 1500°C for pure 8YSZ and 10LSGM and 20LSGM composites. The shrinkage of all specimens started in the 1180°C–1200°C range. Pure 8YSZ exhibited a total shrinkage of ~22%, whereas for composites, it amounted to ~27%. The temperatures corresponding to maximum shrinkage were 1200°C, 1225°C, and 1330°C for 20LSGM, 10LSGM, and pure 8YSZ, respectively. At temperatures higher than 1300°C, the shrinkage of composites slows down.

Table 1 summarizes the relative density data determined after isothermal experiments with a dwell time of 4 h. The relative density of pure 8YSZ after sintering at 1200°C is only 72.5%, but the addition of 10 wt.% LSGM resulted in a significant increase of 22%. The beneficial effect of LSGM on the sintered density of 8YSZ does not hold for temperatures above 1300°C, although for the 1LSGM composite, a small increase in the density in relation to that of pure 8YSZ is observed.

3.2 | Structure and microstructure

Figure 2 depicts SEM micrographs of (A) 8YSZ and (B) 1LSGM composite sintered at 1250°C. The image of pure 8YSZ (Figure 2A) shows small grains, typically less than 1 μm on average in size. Moreover, extensive porosity exists at the grain boundaries, meaning that the sintering process is in the second stage, where pore elimination plays a role. The microstructure of the composite (Figure 2B) consists of polygonal grains with a small volume fraction of porosity compared to that of pure 8YSZ. The porosity in

TABLE 1 Relative density values of pure 8 mol% yttria-stabilized zirconia (8YSZ) and composites sintered at several temperatures for 4 h.

LSGM content (wt.%)	Temperature (°C)	Relative density (± 0.5%)	LSGM content (wt.%)	Temperature (°C)	Relative density (± 0.5%)
-	1200	72.5	-	1350	98.5
1	1200	85.0	1	1350	99.0
10	1200	94.5	10	1350	95.9
20	1200	92.1	20	1350	95.5
-	1250	91.1	-	1400	98.2
1	1250	94.6	1	1400	99.0
10	1250	95.7	10	1400	96.5
20	1250	93.8	20	1400	92.3
-	1300	98.5	-	1450	97.9
1	1300	96.8	1	1450	99.0
10	1300	96.5	10	1450	95.4
20	1300	94.9	20	1450	97.9

Abbreviation: LSGM, $La_{0.9}Sr_{0.1}Ga_{0.8}Mg_{0.2}O_{3-\delta}$.

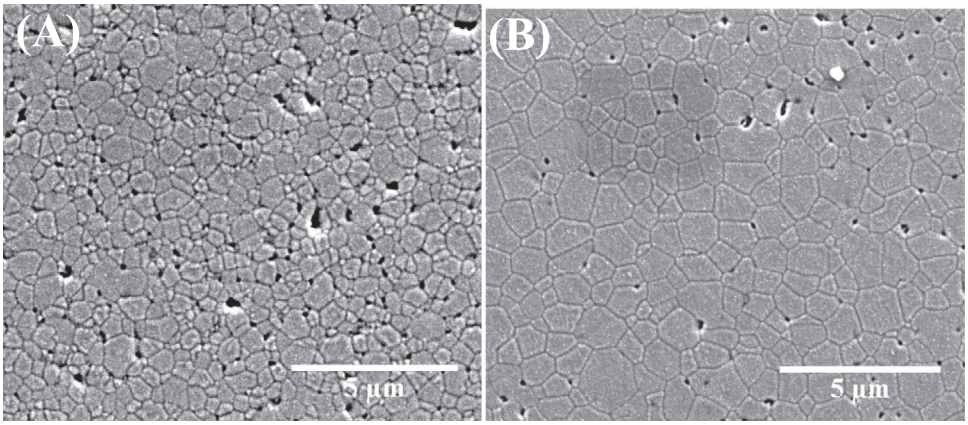

FIGURE 2 Scanning electron microscopic (SEM) micrographs of 8 mol% yttria-stabilized zirconia (8YSZ) sintered at 1250°C/4 h (A) pure and (B) 1 mol% $La_{0.9}Sr_{0.1}Ga_{0.8}Mg_{0.2}O_{3-\delta}$ (1LSGM) composite.

the composite material is mainly found at triple grain junctions, indicating that at 1250°C the composite is at the end of the second stage or at the beginning of the final stage of sintering, with grain growth becoming increasingly significant.

The overall results on dilatometry, density, and microstructure analyses are in general agreement one with each other and suggest that the LSGM addition speeds up the densification kinetics of 8YSZ.

The structure and microstructure evolution of the solid electrolytes were found to be independent of the sintering temperature in the 1300°C–1450°C range. Then, only results in this range will be focused.

The XRD patterns of 8YSZ, LSGM, and composites sintered at 1450°C are shown in Figure 3. Pure materials display the characteristic peaks of the cubic (8YSZ) and orthorhombic (LSGM) structures, indexed according to PDF files 30–1468 and 51–290, respectively. The XRD pattern of 1LSGM is similar to that of 8YSZ, as expected, due to the experimental limitations of the measuring technique. The XRD patterns of the 10LSGM and 20LSGM composites did not exhibit diffraction peaks related to the minor phase. This effect may be due to several factors, such as a large difference in the X-ray absorption coefficient of both materials or the solubility of the minor phase into the matrix, among others. A careful examination of the diffraction patterns reveals a slight shift towards low angles of the diffraction peaks, suggesting some solubility of the minor phase into 8YSZ. The XRD pattern of the 20LSGM composite, in addition, shows low-intensity peaks, indicated by *, characteristics of lanthanum zirconate, $La_2Zr_2O_7$ (PDF 73–444).

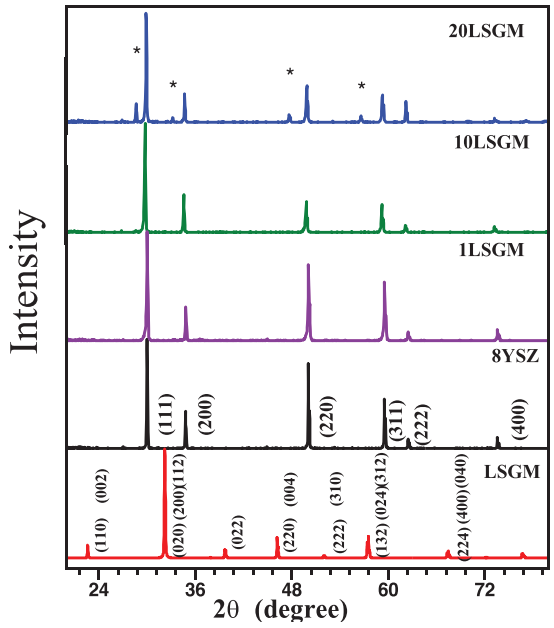

FIGURE 3 X-ray diffraction patterns of pure 8 mol% yttria-stabilized zirconia (8YSZ) and $La_{0.9}Sr_{0.1}Ga_{0.8}Mg_{0.2}O_{3-\delta}$ (LSGM), and composites sintered at 1450°C/4 h. * $La_2Zr_2O_7$ (PDF 73–444).

Figure 4 shows, as an example, SEM micrographs of specimens sintered at 1400°C, when pure 8YSZ as well as the composite materials have achieved their maximum shrinkage.

Pure 8YSZ (Figure 4A) shows polygonal-shaped grains with an average size of 4.2 ± 0.1 μm, and low porosity. The composite 1LSGM (Figure 4B) exhibits a similar microstructure with slightly smaller grains (4.0 ± 0.1 μm average grain size). In contrast, the 10LSGM composite (Figure 4C) is characterized by relatively large grains with 17.5 ± 0.4 μm average size. The SEM micrograph of 20LSGM (Figure 4D) shows a large fraction of the secondary phase. The average grain size is 12.7 ± 0.3 μm. Figure 4E shows a high magnification SEM micrograph of the 10LSGM, revealing submicron sized polygonal grains; those grains are located at triple grain junctions and dispersed along the grain boundaries. Small-sized grains are also observed at triple grain junctions in 1LSGM and 20LSGM composites.

The XRD and SEM results point to a complex microstructure development associated with the LSGM concentration in the 8YSZ matrix. A possible explanation for the observed features is based on both the content and setting of the minor phase. The grains of LSGM are found at triple grain junctions and probably remain as a stable phase for specimens with very low contents, for example ≤ 1 wt.%. The buildup of the submicron grains at the grain boundaries occurs with an increasing fraction of LSGM in the matrix. At this point, two events may take place: solid solution formation and diffusion of zirconium and lanthanum ions leading to the lanthanum zirconate secondary phase. Solid solution should take place first, explaining the large average grain size of 10LSGM and the shift toward small angles in the XRD pattern. An increase of the lanthanum zirconate phase is observed with an additional increment of the LSGM content, probably above the solubility limit. The secondary phase ($La_2Zr_2O_7$) may inhibit, to some extent, the grain growth of the composite.

This picture may, however, be oversimplified, because it does not take into account the well-known diffusion of magnesium ions toward the grain boundaries, neither the loss of gallium from the bulk during high-temperature heat treatments. Then, EDS analyses by elemental mapping and line scan of selected microregions of 10LSGM were carried out to identify the possible contribution of cation diffusion.

Figure 5 shows the SEM image of a specific microregion and the corresponding elemental mapping.

Oxygen (red) is found throughout the entire microregion. Zirconium (pink) and yttrium (cyan) are found in the bulk of the grains. Strontium (green) is also preferentially set up in the bulk. Lanthanum (light blue), magnesium (light purple) and gallium (dark purple) are mostly found at the grain boundaries. Note that the relative concentration of magnesium and gallium goes in the opposite direction so that, the darker is the purple color, the lower is the content of magnesium and the higher is the fraction of gallium. The arrow points to a grain boundary in which some enrichment of oxygen is found, along with magnesium, lanthanum, and gallium.

Figure 6 shows a selected microregion with high magnification (top) and the line scan (bottom) according to the direction of the arrow (top). At both extremes of the arrow, zirconium (brown) and yttrium (black) dominate the spectrum. The white areas crossed by the arrow consist of zirconium, yttrium and lanthanum (olive), suggesting lanthanum zirconate formation. Near the center of the arrow, a grain boundary microregion with gray color shows abrupt reduction of zirconium and yttrium, and a simultaneous growth of the magnesium (green), gallium (blue) and oxygen (red) signals.

Similar results were obtained as well for the 20LSGM composite and suggest that besides the lanthanum gallate secondary phase, diffusion of magnesium and gallium from the bulk towards the grain boundaries promoted another secondary phase, possibly magnesium gallate. Nevertheless, the content of this phase is too small to be detected by conventional X-ray diffraction.

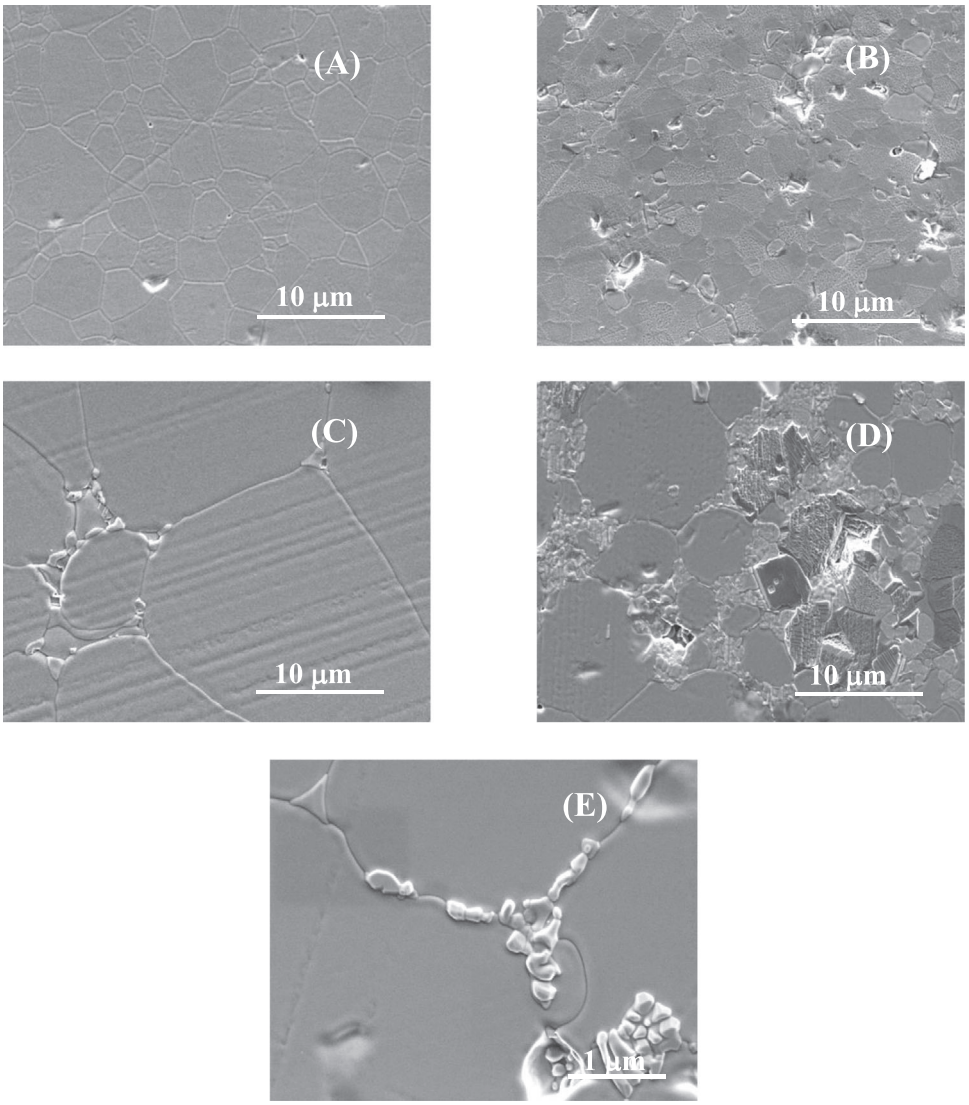

FIGURE 4 Scanning electron microscopic (SEM) micrographs of (A) pure 8 mol% yttria-stabilized zirconia (8YSZ), (B) 1LSGM, (C) 10LSGM, (D) 20LSGM and (E) 10LSGM with high magnification, composites sintered at 1400°C. LSGM, $La_{0.9}Sr_{0.1}Ga_{0.8}Mg_{0.2}O_{3-\delta}$.

3.3 | Electrical and mechanical characterization

The electrical and mechanical characterizations were carried out in specimens sintered at 1450°C, usually employed for sintering of the matrix.

Impedance spectroscopy diagrams of pure 8YSZ and composites are depicted in Figure 7. The -Z''(ω) × Z'(ω) plots recorded at 340°C consist of a sequence of arcs representing the resistive and capacitive effects of bulk and grain boundaries/interfaces. The numbers in the impedance diagrams are the relaxation frequency, and the real and the imaginary components of the total impedance were normalized for sample dimensions for comparison. The arc related to the interfaces/grain boundaries is barely seen in these plots, because of the relatively large average grain sizes.[26] The impedance diagram of 20LSGM shows an overlap of two arcs, probably related to the matrix and to the secondary phases.

The Arrhenius plots of the bulk conductivity, σ_b, for specimens sintered at 1450°C are shown in Figure 8. All specimens display a single straight line with apparent activation energy for conduction of approximately 1 eV. The highest value of the electrical conductivity was obtained for pure LSGM and the lowest for the 20LSGM composite. Extrapolated values of the bulk conductivity of composites at 600°C are 9.45 (1LSGM), 1.61 (10LSGM) and 0.674 $mS.cm^{-1}$ (20LSGM), and 28 (LSGM) and 16.4 $mS.cm^{-1}$ (8YSZ) for pure ceramics. According to the present results, the addition of LSGM in the 1 to 20 wt.% to 8YSZ exerts a deleterious effect on the electrical conductivity

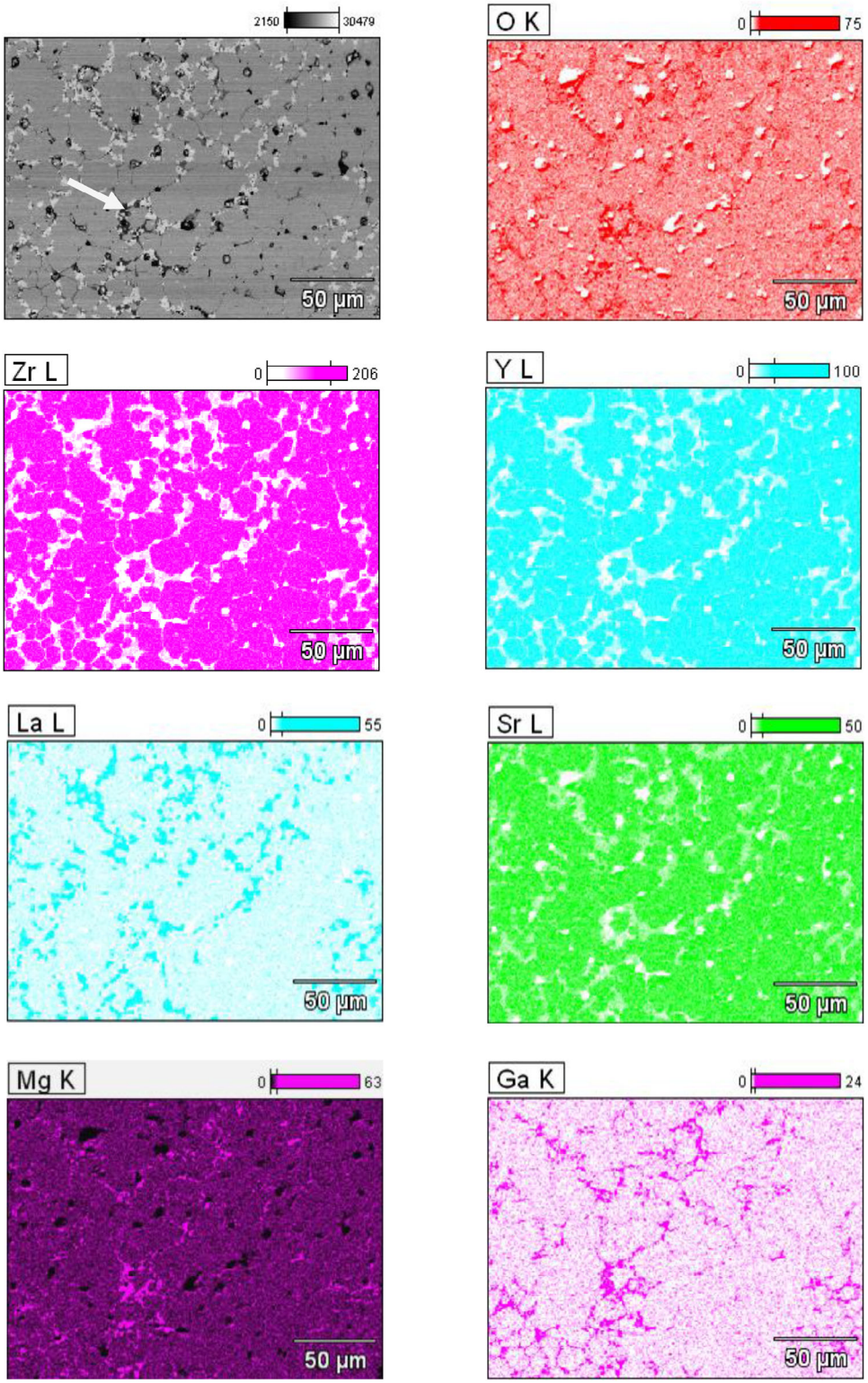

FIGURE 5 Scanning electron microscopic (SEM) micrographs and elemental mapping of a selected microregion of 10LSGM. LSGM, $La_{0.9}Sr_{0.1}Ga_{0.8}Mg_{0.2}O_{3-\delta}$.

TABLE 2 Values of elastic modulus (E) and hardness of 8 mol% yttria-stabilized zirconia (8YSZ), LSGM and 10LSGM and 20LSGM composites sintered at 1450°C. LSGM, $La_{0.9}Sr_{0.1}Ga_{0.8}Mg_{0.2}O_{3-\delta}$.

Material	Load (mN)	E (GPa)	Hardness (GPa)	Load (mN)	E (GPa)	Hardness (GPa)
8YSZ	4	247 ± 3	19.1 ± 0.5	8	241 ± 5	18.2 ± 0.3
LSGM	4	221 ± 2	13.5 ± 0.3	8	206 ± 9	13.6 ± 0.4
10LSGM	4	258 ± 3	18.5 ± 0.5	8	255 ± 2	18.4 ± 0.3
20LSGM **Hard phase**	4	261 ± 2	18.4 ± 0.2	8	257 ± 5	18.2 ± 0.4
20LSGM **Soft phase**	4	234 ± 6	15.3 ± 0.2	8	223 ± 9	15.5 ± 0.1

Abbreviations: LSGM, $La_{0.9}Sr_{0.1}Ga_{0.8}Mg_{0.2}O_{3-\delta}$; YSZ, yttria-stabilized zirconia.

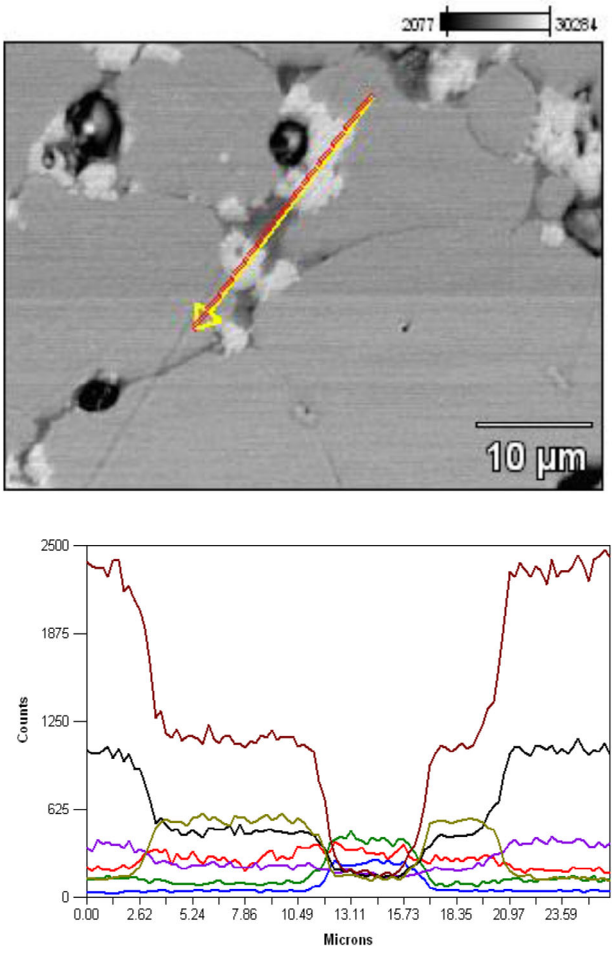

FIGURE 6 Scanning electron microscopic (SEM) micrograph and line scan spectrum of a specific microregion of 10LSGM. Zr-brown; Y-black; La-olive; Sr-purple; Mg-green; Ga-blue; O-red.

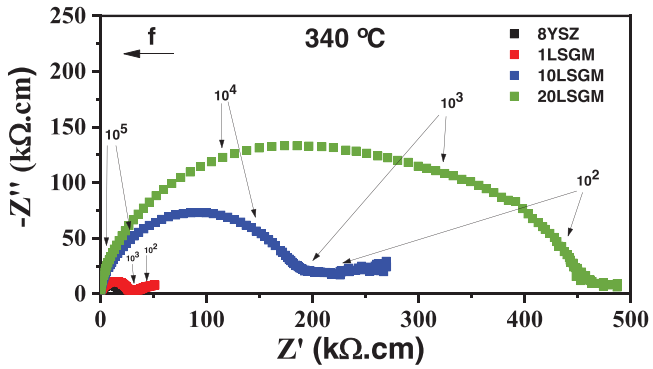

FIGURE 7 Impedance spectroscopy diagrams of pure 8 mol% yttria-stabilized zirconia (8YSZ), and 1LSGM, 10LSGM and 20LSGM composites sintered at 1450°C. LSGM, $La_{0.9}Sr_{0.1}Ga_{0.8}Mg_{0.2}O_{3-\delta}$.

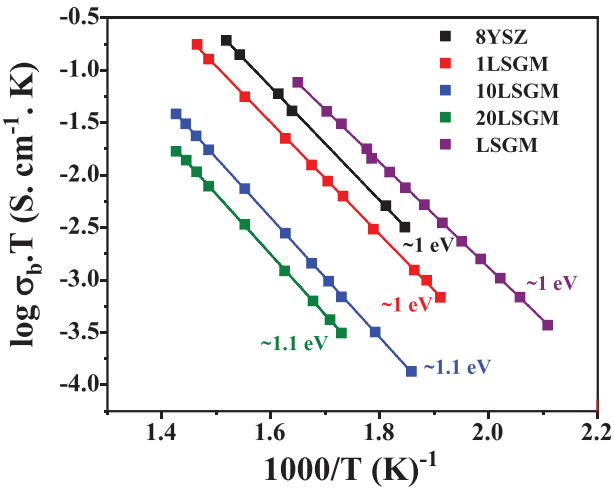

FIGURE 8 Arrhenius plots of the bulk conductivity for 8 mol% yttria-stabilized zirconia (8YSZ), LSGM, and composites sintered at 1450°C. LSGM, $La_{0.9}Sr_{0.1}Ga_{0.8}Mg_{0.2}O_{3-\delta}$.

of 8YSZ attributed to interface reactions occurring during sintering.

Nanoindentation tests allowed observing interesting results based on load–displacement (P–h) curves. The obtained hardness and elastic moduli are summarized in Table 2. A comparison between pure materials (8YSZ and LSGM) reveals that the matrix is harder than the minor phase. Surprisingly, an improvement in the elastic modulus was obtained for the 10LSGM composite, and the hardness was approximately the same as that of 8YSZ. Increasing the volume fraction of LSGM, two distinct behaviors were observed on the load-displacement curve,

denoted in Table 2 as hard and soft phases. The hard phase exhibited similar hardness to 8YSZ and 10LSGM, and a slightly higher elastic modulus than 10LSGM. The soft phase, possibly associated with secondary phases, showed lower hardness and elastic modulus than 8YSZ, but its hardness was higher than that of pure LSGM.

4 | CONCLUSIONS

Composites of 8YSZ and LSGM were successfully obtained via solid state sintering. The addition of the minor phase enhanced the sintering kinetics of the matrix, allowing for obtaining high density values at relatively lower temperatures. Lanthanum zirconate secondary phase was detected in the composite containing 20 wt.% LSGM. The evolution of the microstructure was complex and depended on the relative amount of the minor phase. Enrichment of magnesium and gallium was found at grain boundaries by energy dispersive spectroscopy mapping and line scan. The electrical conductivity of composites is lower than that of 8YSZ and LSGM pure materials. The hardness of the composites was similar to that of pure 8YSZ up to 10 wt.% LSGM. An improved elastic modulus was obtained for the 10LSGM composite.

The overall results highlight that sometimes unpredictable effects may come out when combining ceramic materials because of the several reasons such as point defects, solubility, and interface reactions, among others. Therefore, optimization of solid electrolyte properties is not an easy task and should be investigated deeply, taking into account the potential reactions that may take place during processing and/or further procedures.

ACKNOWLEDGMENTS

This work was supported by FAPESP (2013/07692-2), CNPq (305557/2022-0 and 306894/2023-8), CAPES (Finance code 0001) and CNEN.

ORCID

V. Seriacopi https://orcid.org/0000-0002-1903-867X
Reginaldo Muccillo https://orcid.org/0000-0002-8598-279X
Eliana N. S. Muccillo https://orcid.org/0000-0001-9219-388X

REFERENCES

1. Minh NQ. Ceramic fuel cells. J Am Ceram Soc. 1993;76:563–88. https://doi.org/10.1111/j.1151-2916.1993.tb03645.x
2. Singhal SC. Solid oxide fuel cells for stationary, mobile and military applications. Solid State Ionics. 2002;152:405–10. https://doi.org/10.1016/S0167-2738(02)00349-1
3. Ghatee M, Shariat MH, Irvine JTS. Investigation of electrical and mechanical properties of 3YSZ/8YSZ composite electrolytes. Solid State Ionics. 2009;16:57–62. https://doi.org/10.1016/j.ssi.2008.10.006
4. Ishihara T, Honda M, Takita Y. Doped $LaGaO_3$ perovskite type oxide as a new oxide ionic conductor. J Am Chem Soc. 1994;116:3801–3. https://doi.org/10.1021/ja00088a016
5. Morales M, Roa JJ, Tartaj J, Segarra M. A review of doped lanthanum gallates as electrolytes for intermediate temperature solid oxides fuel cells: from materials processing to electrical and thermo-mechanical properties. J Eur Ceram Soc. 2016;36:1–16. https://doi.org/10.1016/j.jeurceramsoc.2015.09.025
6. Fonseca FC, Florio DZde, Esposito V, Traversa E, Muccillo ENS, Muccillo R. Mixed ionic-electronic YSZ/Ni composite for SOFC anodes with high electrical conductivity. J Electrochem Soc. 2006;153:A354–60. https://doi.org/10.1149/1.2149312
7. Huang B, Zhu XJ, Hu WQ, Wang YY, Yu QC. Characterization of the Ni-ScSZ anode with LSCM-CeO_2 catalyst layer in thin film solid oxide fuel cell running on ethanol fuel. J Power Sources. 2010;195:3053–9. https://doi.org/10.1016/j.jpowsour.2009.11.126
8. Lu LH, Shi QL, Yang Y, Zhang H. Electrochemical performance of $(La,Sr)(Co,Fe)O_{3-\delta}$-$(Ce,Sm)O_{2-\theta}$-CuO composite cathodes for intermediate temperature solid oxide fuel cells. Mater Res Bull. 2012;47:1016–20. https://doi.org/10.1016/j.materresbull.2012.01.005
9. Porotnikova N, Khrustov A, Farlenkov A, Khodimchuk A, Partin G, Animitsa I, et al. Promising $La_2Mo_2O_9$ - $La_2Mo_3O_{12}$ composite oxygen—ionic electrolytes: interphase phenomena. ACS Appl Mater Interfaces. 2022;14:6180–93. https://doi.org/10.1021/acsami.1c20839
10. Guseva A, Pestereva N, Uvarov N. New oxygen ion conducting composite solid electrolytes $Sm_2(WO_4)_3$-WO_3. Solid State Ionics. 2023;394:116196. https://doi.org/10.1016/j.ssi.2023.116196
11. Liu C, Zhang H, Xia J, Li Z. Synthesis and characterization of $Zr_{0.85}Y_{0.15}O_{1.925}$-$La_{9.33}Si_6O_{26}$ composite electrolyte for application in SOFCs. J Adv Ceram. 2012;1:327–35. https://doi.org/10.1007/s40145-012-0033-x
12. Maurya R, Gupta A, Omar S, Balani K. Effect of sintering on mechanical properties of ceria reinforced yttria-stabilized zirconia. Ceram Int. 2016;42:11393–403. https://doi.org/10.1016/j.ceramint.2016.04.069
13. Raghvendra PS. Electrical conductivity of YSZ-SDC composite solid electrolyte synthesized via glycine-nitrate method. Ceram Int. 2017;43:11692–8. https://doi.org/10.1016/j.ceramint.2017.05.359
14. Nie JJ, Zheng D, Ganesh KS, Akbar M, Xia C, Dong WJ, et al. Efficient strategy to boost the electrochemical performance of yttrium-stabilized zirconia electrolyte solid oxide fuel cell for low-temperature applications. Ceram Int. 2021;47:3462–72. https://doi.org/10.1016/j.ceramint.2020.09.190
15. Liu K, Bai Y, Li JR, Ma J, Du JG, Cao Y, et al. Structure-property relationship and design of plasma-sprayed $La_2Ce_2O_7$/8YSZ composite coatings for gas turbine blades. Ceram Int. 2018;44:13662–73. https://doi.org/10.1016/j.ceramint.2018.04.204
16. Zhang J, Guo XY, Zhang Y, Lu Z, Choi HH, Jung YG, et al. Mechanical properties of lanthanum zirconate based composite thermal barrier coatings. Adv Appl Ceram. 2019;118:257–63. https://doi.org/10.1080/17436753.2018.1564415

17. Fernandes CM, Castela A, Figueiredo FM, Frade JR. Microstructure-property relations in composite yttria-substituted zirconia solid electrolytes. Solid State Ionics. 2011;193:52–9. https://doi.org/10.1016/j.ssi.2011.02.017
18. Liu LF, Cheng YH, Wei WCJ. Processing of high conductivity Bi_2O_3/8YSZ composites as SOFC electrolyte. J Ceram Process Res. 2019;20:347–56.
19. Tian Y, Liu S, Zhang X, Xiao S, Sun J, Zhang J, et al. Controlled synthesis of Bi_2O_3-YSZ composite powders and their sintering behavior for high-performance electrolytes. Int J Appl Ceram Technol. 2023;20:1398–407. https://doi.org/10.1111/ijac.14270
20. Mihn NQ. Ceramic fuel cells. J. Am. Ceram. Soc. 1993;76:563–88. https://doi.org/10.1111/j.1551-2916.1993.tb03645.x
21. Chen A, Bourne G, Siebein K, DeHoff R, Wachsman E, Jones K. Characterization of lanthanum zirconate formation at the A-site-deficient strontium-doped lanthanum manganite cathode/yttrium-stabilized zirconia electrolyte interface of solic oxide fuel cells. J. Am. Ceram. Soc. 2008;91:2670–5. https://doi.org/10.1111/j.1551-2916.2008.02524.x
22. Fujimoto TG, Reis SL, Muccillo ENS. Influence of yttria-stabilized zirconia on microstructure and electrical properties of doped lanthanum gallate. Mater Res. 2019;22:e20190043. https://doi.org/10.1590/1980-5373-MR-2019-0043
23. Reis SL, Muccillo ENS. Preparation of dense $La_{0.9}Sr_{0.1}Ga_{0.8}Mg_{0.2}O_{3-\delta}$ with high ionic conductivity by solid-state synthesis. Ionics. 2018;24:1693–700. https://doi.org/10.1007/s11581-017-2344-y
24. Kleitz M, Kennedy JH. Resolution of multicomponent impedance diagrams. In: Mundy JN, Shenoy GK, Vashishta P, editors. Fast ion transport in solids. North-Holland: Elsevier; 1979. p. 185–8.
25. Oliver WC, Phar GM. Measurement of hardness and elastic modulus by instrument indentation: advances in understanding and refinements of methodology. J Mater Res. 2004;19:3–20. https://doi.org/10.1557/jmr.2004.19.1.3
26. Kleitz M, Bernard MH, Fernandez E, Schouler E. Impedance spectroscopy and electrical resistance measurements on stabilized zirconia. In: Heuer AH, Hobbs LW, editors. Science and Technology of Zirconia I. Ohio: The American Ceramic Society; 1981. p. 310–36.

How to cite this article: Fujimoto TG, Seriacopi V, Machado IF, Muccillo R, Muccillo ENS. Physical characterization of composites based on yttria-stabilized zirconia and doped lanthanum gallate. Int J Appl Ceram Technol. 2025;22:e15003. https://doi.org/10.1111/ijac.15003